

PAPER • OPEN ACCESS

Magnetohydrodynamic effects in liquid metal batteries

To cite this article: F Stefani *et al* 2016 *IOP Conf. Ser.: Mater. Sci. Eng.* **143** 012024

View the [article online](#) for updates and enhancements.

You may also like

- [Estimation of aquifer dimensions from passive seismic signals with approximate wave propagation models](#)
Timo Lähivaara, Nicholas F Dudley Ward, Tomi Huttunen et al.
- [Linear Stability Analysis of Transient Electrodeposition in Charged Porous Media: Suppression of Dendritic Growth by Surface Conduction](#)
Edwin Khoo, Hongbo Zhao and Martin Z. Bazant
- [Fast Charging of Energy-Dense Lithium Metal Batteries in Localized Ether-Based Highly Concentrated Electrolytes](#)
Yongjun Leng, Shanhai Ge, Xiao-Guang Yang et al.



ECS
The
Electrochemical
Society
Advancing solid state &
electrochemical science & technology

DISCOVER
how sustainability
intersects with
electrochemistry & solid
state science research

Magnetohydrodynamic effects in liquid metal batteries

**F Stefani, V Galindo, C Kasprzyk, S Landgraf, M Seilmayer, M Starace,
N Weber and T Weier**

Helmholtz-Zentrum Dresden – Rossendorf, Bautzner Landstraße 400, 01328 Dresden,
Germany

E-mail: F.Stefani@hzdr.de

Abstract. Liquid metal batteries (LMBs) consist of two liquid metal electrodes and a molten salt ionic conductor sandwiched between them. The density ratios allow for a stable stratification of the three layers. LMBs were already considered as part of energy conversion systems in the 1960s and have recently received renewed interest for economical large-scale energy storage. In this paper, we concentrate on the magnetohydrodynamic aspects of this cell type with special focus on electro-vortex flows and possible effects of the Tayler instability.

1. Introduction

The increasing deployment of strongly fluctuating renewable energies requires a corresponding large-scale expansion of electricity storage. While electrolytically generated hydrogen, partly processed to synthesized hydrocarbons (power-to-gas, power-to-liquids), is widely considered the only viable way for long-term storage on the TWh scale, electrochemical storage is an attractive candidate for short-term and mid-term storage. Stationary Sodium-Sulfur (NaS) batteries, which are already sold as an industrial product on the MW scale, may have a promising future, in particular if the mass storage of Na and S can be spatially separated from the actual energy converter.

Liquid metal batteries (LMBs) are presently discussed as an alternative route of economical grid-scale energy storage. LMBs had been intensively studied in the 1960s [1], and experience a remarkable renaissance nowadays [2]. They consist of two liquid metal electrodes and a molten salt ionic conductor sandwiched between them. The respective density ratios allow for a stable stratification of the three layers. On discharge, the upper alkaline (Li, Na...) or earth-alkaline (Mg, Ca...) metal is oxidized, and its cations cross the fused salts into the lower layer where they are reduced and alloy with a heavy metal (Pb, Bi...) or metalloid (Sb).

The main advantage of this setup is the ultrafast charge transfer kinetics due to the liquid-liquid electrode-electrolyte interface, and the fast mass transport in liquids, allowing for charging and discharging current densities of about 4-100 kA m⁻² (depending on the choice of the anode, cathode, and electrolyte material). The second advantage is the potentially low cost which results from the abundance of electrode materials such as Na and Pb. Further to this, the absence of any degradation effects due to the use of liquid metals and salts promises unprecedented cycle life.

Disadvantages of LMBs are the comparably low cell voltages (typically < 1 V), high operating temperatures to keep the metals and the salt liquid, several corrosion problems, and high self-discharge rates for some of the used metals (including, unfortunately, Na) due to their significant solubility in the molten salt electrolyte.



In this paper, we will be concerned with another issue. While fluid dynamics does not play any role in most traditional battery systems, it cannot be neglected in LMBs (see Figure 1). It goes without saying that LMBs are not suitable for mobile applications since any acceleration would lead to uncontrollable movements of the three layers and very likely to a rupture of the electrolyte, with possibly drastic consequences due to the resulting heat. But even for stationary applications there are flow-driving energy sources which should be carefully considered. Small batteries, with sufficiently thick electrolytes, have been safely operated for months. The ultimate goal is, however, to construct LMBs as large as possible with electrolyte layers as thin as possible. The latter derives from the demand to minimize the unavoidable voltage loss $V_{\text{loss}} = d j / \sigma$ within the electrolyte of thickness d and conductivity σ , for a charging/discharging current with density j . The former request is a consequence of the (rough) estimate that the active materials costs are (presently) only one fourth (or so) of the total battery costs, and that any increase of the size would lead to a significant decrease of the costs, both per kW and per kWh.

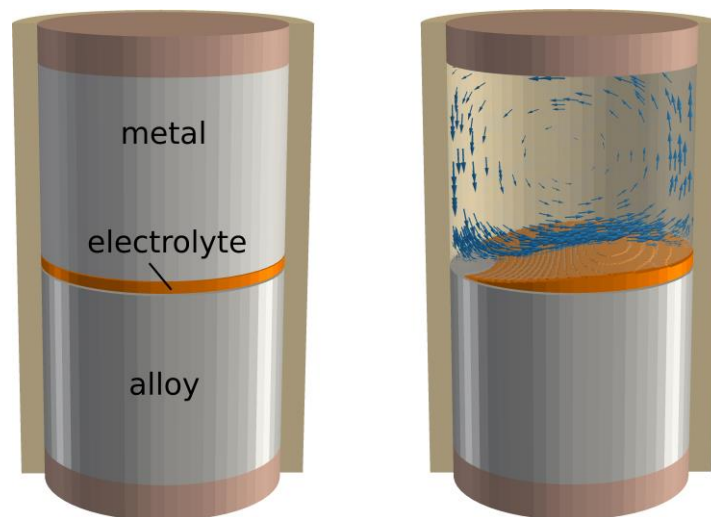


Figure 1. Sketch of a liquid metal battery with typical inventory. The electrolyte, which separates the two liquids, acts as an ion conductor. A strong enough flow might wipe the electrolyte and lead to a short circuit.

This paper deals, therefore, with the following question: what kind of limitations are set by (magneto)-hydrodynamic effects on the maximum size of LMBs and/or on the minimum thickness of the electrolyte layer, and what countermeasures could be taken to overcome those limitations?

2. Magnetohydrodynamics of Liquid Metal Batteries

The full hydrodynamics of LMBs is extremely involved. It includes Rayleigh-Bénard convection due to resistive heating of the electrolyte layer, surface-tension driven flows, capillary effects at the walls etc. Here, we focus on the magnetohydrodynamic (MHD) aspects, including electro-vortex flows and various current-driven instabilities. Even this restricted problem gets rather complex, and includes, e.g. the mutual interaction of current-driven flow instabilities and long and short wave interface instabilities, whose numerical study has just begun.

In the following, we will start to tackle the issue from two sides. We will first discuss the so-called Tayler instability (TI), a kink type current-driven instability, and second the electro-vortex flow (EVF) which appears when current distributions are inhomogeneous. While the latter might indeed be more

relevant for real-world LMBs with their complicated wiring system and current-collectors of finite thickness, the TI still marks a paradigmatic reference point. Actually, for large total currents the TI would lead to vigorous flows, and the ultimate disruption of the electrolyte layer, even in the idealized case that the charging/discharging current could be made perfectly homogeneous. We will also show some first results on the interaction of TI and EVF, and their influence on the metal-salt interface.

2.1. Tayler instability

The kink-type Tayler instability had first been discussed in the context of fusion related and astrophysical plasma physics. The self-interaction of a homogeneous axial current in a cylinder with its own azimuthal magnetic field produces an inwardly directed pinch force that becomes unstable either to an axisymmetric (“sausage”) or to a non-axisymmetric (“kink”) instability. In the idealized case without any viscosity or resistivity of the fluid, the kink instability can be suppressed either by an additional axial magnetic field (leading to the celebrated Kruskal-Shafranov condition of fusion research [3]), by stable stratification [4], or by rotation [5]. Comparably late, the stabilizing effect of viscosity and resistivity was investigated in detail in [6] where the key role of the Hartmann number for the onset of the TI was also identified. This Hartmann number $Ha = B_\phi(R) R (\sigma/\rho\nu)^{1/2}$ (with $B_\phi(R)$ denoting the azimuthal field at cylinder radius R , and σ, ρ, ν denoting conductivity, density, and viscosity of the fluid), which measures the ratio of magnetic forces to viscous forces, must be above 20 for the TI to set in [7]. This critical number, together with typical growth rates of the TI, has recently been confirmed in a liquid metal experiment using electrical currents up to 8 kA [8].

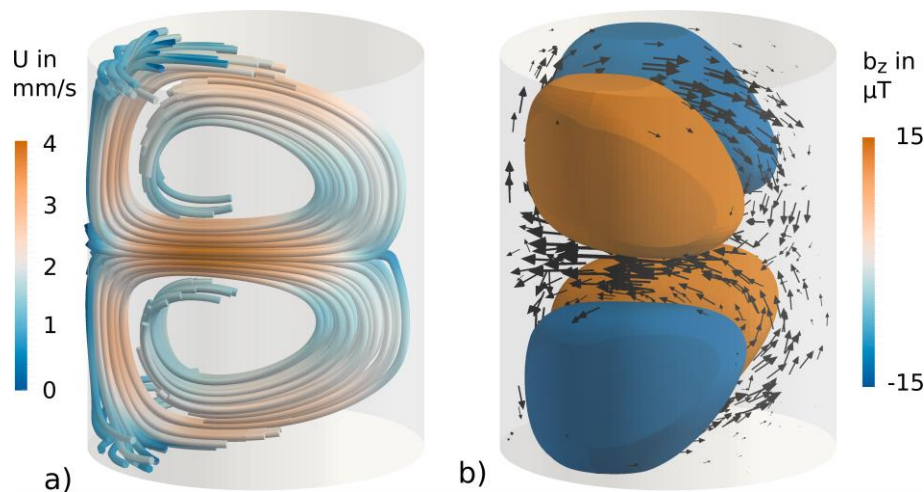


Figure 2. Simulated Tayler instability for a cylinder filled with liquid Li, at a current of 4 kA. (a) Flow structure, (b) induced axial magnetic field component.

In order to simulate the effects of the TI as well as of EVFs on LMBs, we have set up a numerical model [9] on the basis of the OpenFOAM library which is extended by a Poisson solver for the electric potential and an implementation of Biot-Savart’s law for the induced magnetic field. Figure 2 gives a first impression of the TI for the case of a liquid lithium column with a total current of 4 kA. We can easily recognize the asymmetric, kink-type structure of the flow which is, however, superposed by an axisymmetric component arising in the non-linear saturation regime of the TI.

In a follow-up paper [10] we had discussed several means for preventing the TI. The simplest way is to avoid high columns of liquid metals so that the TI, which appears with a typical wavelength, cannot develop within the limited height. However, this height constraint represents a limitation of the storable electric energy. As a rough estimate, valid for Na and a current density of 10 kA m^{-2} , one hour

corresponds to 1 cm. If one plans to store energy for a few days, one easily ends up with heights in the order of 1 m.

Three alternative methods to suppress the TI are sketched in figure 3. A return current through a central bore changes the radial structure of the azimuthal field in such a way that the TI disappears [12]. An axial magnetic field B_z suppresses the TI according to the Kruskal-Shafranov condition [3]. Note, however, that this additional B_z can give rise to a sloshing motion of the interface, as it is known from aluminium reduction cells. A slight stabilization could also be achieved by applying a horizontal magnetic field B_x .

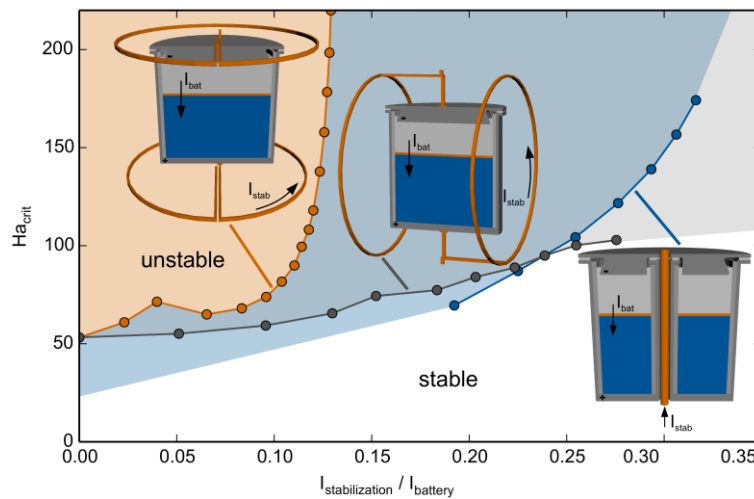


Figure 3. Three methods of suppressing the TI in liquid metal batteries. A return current through a central bore changes the radial structure of azimuthal field in such a way that the TI disappears. An additional axial magnetic field B_z suppresses the TI according to the Kruskal-Shafranov condition. A similar effect is achieved by a horizontal field B_x .

2.2. Electro-vortex flow

We consider now the case that the electrical current is not completely homogeneous. This is already relevant if the current collectors above and below the battery have a finite length (which is always the case). Imagine that this finite-length battery is connected to wires, the current will acquire radial components which are still present in the parts of the fluid close to the collectors. Despite their smallness compared to the total current, these radial components together with the azimuthal field produce a Lorentz force that points away from the current collectors. The resulting EVF will compete with the TI in a non-trivial manner [11].

For a simplified geometry, this is illustrated in Figure 4 where we distinguish three cases. In the first case, “fixed potential over D ”, the effect of the current collectors is simply neglected and it is assumed that the applied current is completely homogeneous in the fluid. Then, the TI develops as usual. If we now consider a current collector of height $h=3D$, with a constant potential applied over a circular diameter $d=D/2$, we see that initially an EVF is developing, with its typical (more or less axisymmetric) double-vortex structure driven by the Lorentz forces close to the current collectors. After some time, however, the TI comes into play and drives the systems to velocities which are slightly larger than the usual ones. If we decrease the height of the current collectors to $h=2D$, the EVF develops faster, and reaches such velocities which apparently lead to suppression of the TI. Obviously the interaction of TI and EVF is quite intricate.

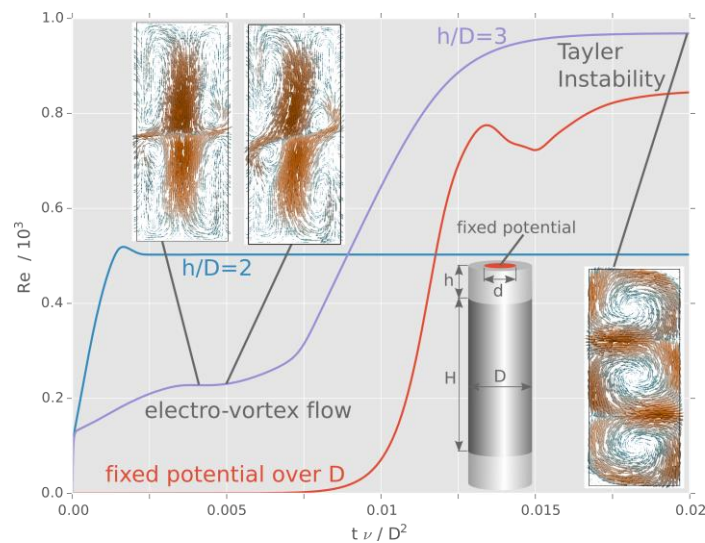


Figure 4. Interaction of TI and EVF. Mean velocity in a cylindrical liquid metal column ($D = 1$ m, $H = 2.4$ m) for an applied current corresponding to $Ha = 100$. Simulation is carried out without current collector and a current collector of aspect ratio 2 or 3 with an electrical conductivity 5 times larger than that of the fluid.

2.3. EVF and the integrity of the electrolyte layer

Let us focus now on the case of a pure EVF, and consider its effect on the multiphase stratification in a real battery. For this purpose, we consider a Na-Bi system with a molten salt as electrolyte. The current collectors are assumed as rather thin so that a very vigorous EVF appears. The shape of the electrolyte layer is computed by a volume-of-fluids (VOF) method. Figure 5 shows the time evolution of the EVF and the salt layer. From the thickness of the salt layer we can infer at which current the layer is disrupted.

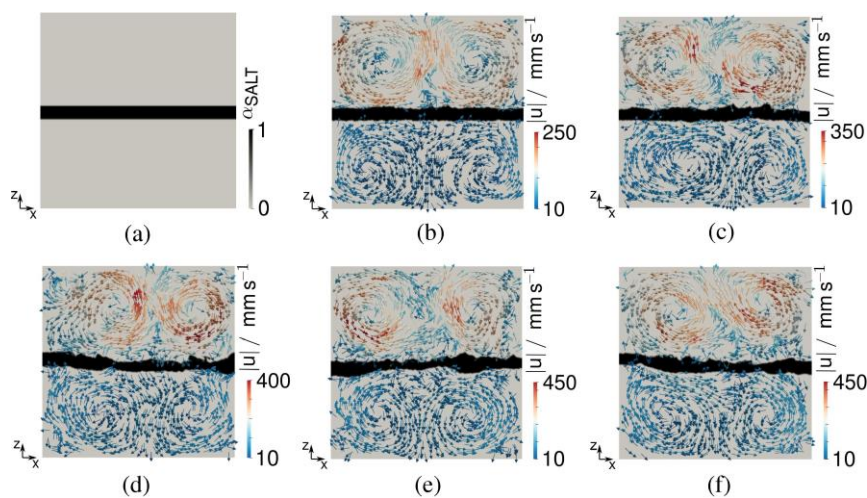


Figure 5. Time evolution of the flow and the electrolyte layer for an EVF in a cell with aspect ratio 1. The snapshots (a-f) correspond to the instants 0, 4 s, ..., 20 s, respectively. Initially, the thickness of the salt layer is 0.09 of the total height. The current is 1 kA.

Taking into account possible real current densities in LMBs, we then change the electrical current and the initial thickness h_0 of the salt layer to obtain a variety of combinations of relevant parameters. Motivated by [13], we expect that the governing parameter for the integrity of the layer is the Richardson number $Ri_{Na} = (\rho_{salt} / \rho_{Na} - 1) g h_0 / \langle v_{Na} \rangle^2$ which is the ratio of the potential energy to the kinetic energy (g is the gravitational acceleration, and $\langle v_{Na} \rangle$ is the averaged velocity magnitude in the Na layer). Figure 6 confirms that this is indeed the case: approximately at $Ri_{Na}=1$, the minimum layer thickness bends sharply to zero and the risk of a potential battery failure increases.

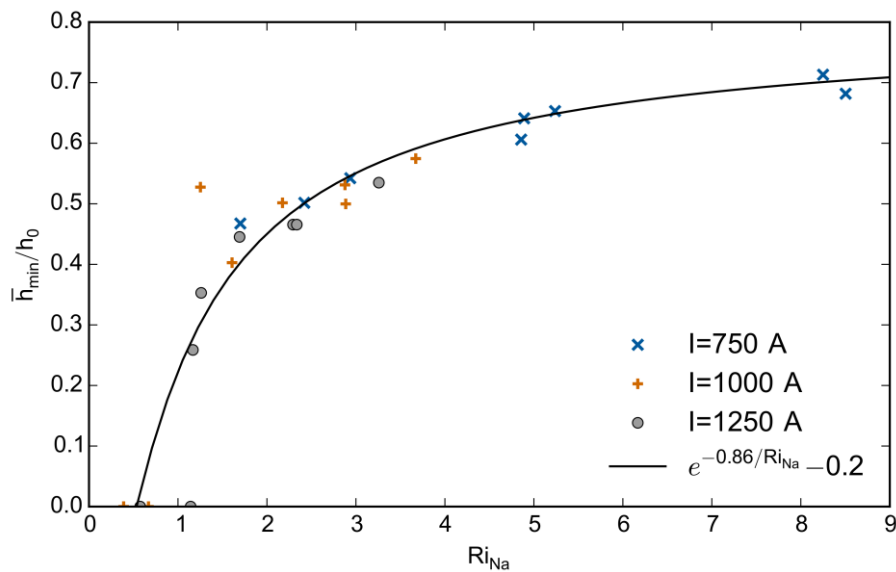


Figure 6. Dependence of the normalized minimal thickness of the salt layer on the Richardson number for Na. The solid line corresponds to a fit with an exponential function.

3. Towards a real battery

In this section, we show the very first results of a small LMB experiment carried out at HZDR. We have chosen the traditional Na-Bi system, but have replaced the pure Na-salts by the mixture LiCl-KCl-NaCl, mainly for reasons of its lower melting temperature. Figure 7 shows the experimental set-up, including a copper vessel filled with Bi at the bottom, and the salt on top of it. The central position of the Na drop at the top is guaranteed by holding it with a Ta wire. Figure 7 also shows the voltage versus time upon charge and discharge. The thickness of the electrolyte is approximately 4 mm. The interface area between the electrolyte and the sodium drop is not very precisely known. A reasonable estimate is one half of the surface of the sphere. In any case, with measured currents of 300 mA, we obtain a remarkable current density in the order of 10 kA m^{-2} .

4. Conclusions and prospects

In this paper, we have discussed some particular aspects of the complex (magneto)-hydrodynamics of LMBs. We have started with the idealized setting of a perfectly homogeneous current, which becomes prone to the TI if the total current increases to a value that corresponds to a Hartmann number in the order of 20. In this context, we have discussed various means for the suppression of the TI. The consideration of EVF has shown that even minor deviations from the idealized homogenous current assumption can lead to vigorous flows. A first simulation of a simplified three-layer system confirmed

the relevance of the Richardson number for integrity of the stratification, which was already discussed in [14]. Some very preliminary experimental results with a Na-Bi battery system, using a LiCl-KCl-NaCl electrolyte, have reassured that current densities in the order of 10 kA m^{-2} are indeed realistic.

The way to a competitive, large-scale LMB is still long, and will need a close collaboration of chemistry, numerics, and advanced engineering. Hopefully, large-scale LMBs will soon be set up and tested in the framework of the DRESLYN project at HZDR [15].

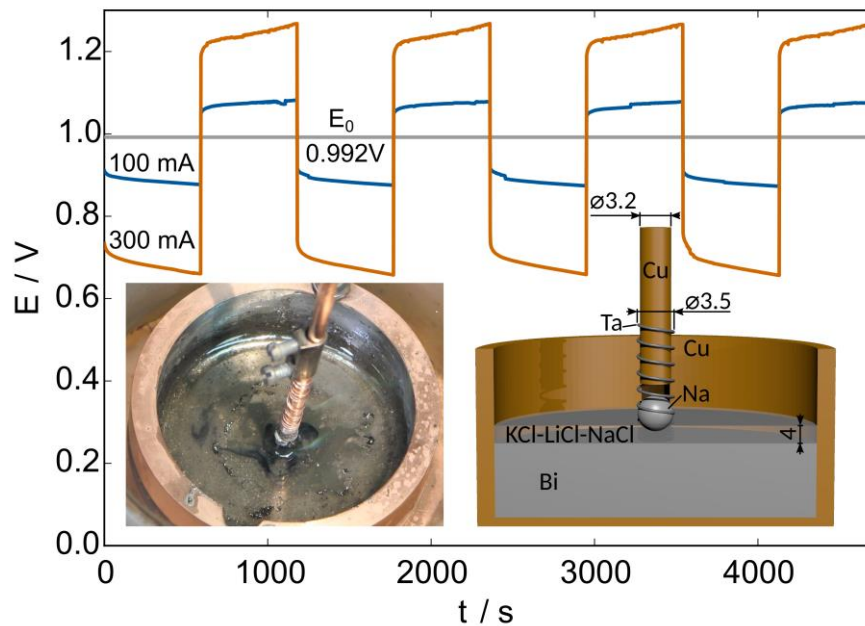


Figure 7. A real battery with Na-Bi and KCl-LiCl-NaCl as electrolyte, and the voltage versus time upon charging/discharging.

5. Acknowledgments

This work was supported by Helmholtz-Gemeinschaft Deutscher Forschungszentren (HGF) in frame of the Helmholtz Alliance LIMTECH, as well as by Deutsche Forschungsgemeinschaft in frame of the SPP 1488 (“PlanetMag”). Fruitful discussions with Wietze Herreman, Caroline Nore, and Janis Priede are gratefully acknowledged.

6. References

- [1] Cairns EJ and Shimotake H 1969 *Science* **164** 1347
- [2] Kim H et al. 2013 *Chem. Rev.* **113** 2075
- [3] Kruskal M and Tuck J 1958 *Proc R. Soc. A* **245** 222
- [4] Tayler RJ 1973 *Mon. Not. R. Astron. Soc.* **161** 365
- [5] Pitts E and Tayler RJ 1985 *Mon. Not. R. Astron. Soc.* **216** 139
- [6] Spies GO 1988 *Plasma Phys. Control. Fusion* **30** 1025
- [7] Rüdiger G, Schultz M and Gellert M 2011 *Astron. Nachr.* **10** 1
- [8] Seilmayer M et al 2012 *Phys. Rev. Lett.* **108** 244501
- [9] Weber N, Galindo V, Stefani F, Weier T and Wondrak T 2013 *New J. Phys.* **15** 043034
- [10] Weber N, Galindo V, Stefani F and Weier T 2014 *J. Power Sources* **265** 166
- [11] Weber N, Galindo V, Priede J, Stefani F and Weier T 2015 *Phys. Fluids* **27** 014103

- [12] Stefani F, Weier T, Gundrum T and Gerbeth G 2011 *Energy Convers. Manag.* **52** 2982
- [13] Banks RB and Bhavamai A 1965 *J. Fluid Mech.* **23** 229
- [14] Herreman W, Nore C, Cappanera L and Guermond J-L 2015 Tayler instability in liquid metal columns and liquid metal batteries 2015 *J. Fluid Mech.* **771** 79
- [15] Stefani F et al. 2012 *Magnetohydrodynamics* **48** 103